JOURNAL OF
NEUROIMAGING
THE OFFICIAL JOURNAL OF THE AMERICAN SOCIETY OF NEUROIMAGING

WILEY

An Automated Algorithm for Optic Nerve Sheath Diameter Assessment from B-mode Ultrasound Images

Raoul R. F. Stevens[1] | Wouter Huberts[2,3] | Erik D. Gommer[4] | Michael Ertl[5] | Marcel Aries[6] | Werner H. Mess[4] | Tammo Delhaas[2]

[1] Department of Biomedical Engineering, MHeNs School for Mental Health and Neuroscience, Maastricht University, Maastricht, The Netherlands

[2] Department of Biomedical Engineering, CARIM School for Cardiovascular Diseases, Maastricht University, Maastricht, The Netherlands

[3] Department of Biomedical Engineering, Eindhoven University of Technology, Eindhoven, The Netherlands

[4] Department of Clinical Neurophysiology, Maastricht University Medical Centre, Maastricht, The Netherlands

[5] Department of Neurology and Clinical Neurophysiology, University Hospital Augsburg, Augsburg, Germany

[6] Department of Intensive Care, Maastricht University Medical Centre, Maastricht, The Netherlands

Correspondence
Raoul R. F. Stevens, Department of Biomedical Engineering, MHeNs School for Mental Health and Neuroscience, Maastricht University, 6200 MD Maastricht, The Netherlands.
Email: raoul_stevens@hotmail.com

ABSTRACT

BACKGROUND AND PURPOSE: The optic nerve sheath diameter (ONSD) is a promising surrogate marker for the detection of raised intracranial pressure (ICP). However, inconsistencies in manual ONSD assessment are thought to affect ONSD and the corresponding ONSD cutoff values for the diagnosis of elevated ICP, hereby hampering the full potential of ONSD. In this study, we developed an image intensity-invariant algorithm to automatically estimate ONSD from B-mode ultrasound images at multiple depths.

METHODS: The outcomes of the algorithm were validated against manual ONSD measurements by two human experts. Each expert analyzed the images twice (M1 and M2) in unknown order.

RESULTS: The algorithm proved capable of segmenting the ONSD in 39 of 42 images, hereby showing mean differences of $-.08 \pm .45$ and $-.05 \pm .41$ mm compared to averaged ONSD values (M1 + M2/2) of Operator 1 and Operator 2, respectively, whereas the mean difference between the two experts was $.03 \pm .26$ mm. Moreover, differences between algorithm-derived and expert-derived ONSD values were found to be much smaller than the 1 mm difference that is expected between patients with normal and elevated ICP, making it likely that our algorithm can distinguish between these patient groups.

CONCLUSIONS: Our algorithm has the potential to improve the accuracy of ONSD as a surrogate marker for elevated ICP because it has no intrinsic variability. However, future research should be performed to validate if the algorithm does indeed result in more accurate noninvasive ICP predictions.

KEYWORDS
Algorithm, intracranial pressure, ONSD, ultrasound

INTRODUCTION

The optic nerve sheath diameter (ONSD) is a promising surrogate marker for noninvasive estimation of intracranial pressure (ICP)[1–6] and is therefore often measured in clinical practice. The ONSD is manually assessed from ultrasound B-mode images, mostly at a depth of 3 mm from the papilla because that region is assumed to be most sensitive to changes in ICP.[7] Although intra- and interobserver variability in ONSD estimation can be low within individual studies,[8,9] ONSD cutoff values for the diagnosis of elevated ICP (>15 mmHg) vary between studies.[10–13] A possible explanation could be discrepancies in ONSD assessment methodologies between different centres[12–14] and discrepancies in the interpretation of the echoic behavior of the different layers of the optic nerve sheath.[12,15,16] Although ONSD assessment might be improved by standardization according to respective guidelines, ONSD values would still be dependent on the compliance

of operators. Differences in manual ONSD measurements might be overcome by constructing an automated framework for ONSD assessment. Automated approaches on ONSD segmentation from ultrasound images have already been reported in literature.[17–19] In contrast to Gerber et al[17] and Soroushmehr et al,[18] Meiburger et al[19] developed an algorithm that was able to segment the outlines of both the optic nerve and the optic nerve sheath instead of determining only a single ONSD value at a depth of 3 mm, thereby opening possibilities to investigate the sensitivity of ONSD to changes in ICP at multiple depths.

Although the approach by Meiburger et al[19] is promising, we observed that our ocular ultrasound images displayed a less clear distinction between the hyperechoic bands and the retrobulbar fat in 37 of 42 images. Hence, detecting the outline of the hyperechoic bands using intensity thresholds as proposed by Meiburger et al[19] would be difficult in our images. Moreover, image intensities and contrast can differ between ultrasound images due to, for example, differences in ultrasound machine settings, which might hamper the applicability of intensity-based algorithms when deployed in different clinical centres. In this study, we therefore developed and evaluated an automatic ONSD algorithm that is less dependent on differences in image intensities.

METHODS

Image acquisition and patient data

A total of 42 B-mode transocular ultrasound images were acquired from 26 comatose patients suffering from traumatic brain injury or subarachnoid hemorrhage who were admitted to the intensive care unit of the Maastricht University Medical Centre (Maastricht, the Netherlands). The study was approved by the local ethical committee (METC 16-04-243) and written informed consent was obtained for all participants. Images were acquired with a Philips iU22 ultrasound device (Eindhoven, The Netherlands) and a 17-5 MHz linear transducer by two investigators.

Measurements were performed on both eyes (if possible) by placing the transducer horizontally on the closed eyelid with the patient in supine position and the head tilted at an angle of 20-30°. The transducer angle was adjusted to find the best possible image of the optic nerve, that is, the optic nerve in a vertical orientation with the hyperechoic bands visible on both sides of the nerve. To prevent tissue damage, the mechanical index (MI) was always kept lower than .3. Finally, the images were exported from the ultrasound machine to a computer for offline assessment.

Automated algorithm

The algorithm was developed in Matlab (R2018a, The MathWorks, Inc., Natick, Massachusetts, United States) and consists of six consecutive steps:

- Step 1: Automatic cropping;
- Step 2: Image enhancement;
- Step 3: Feature calculation;
- Step 4: Initial fat and sheath detection;
- Step 5: Segmentation of the outline using an active contour; and
- Step 6: ONSD calculation.

### Step 1: Automatic cropping

To facilitate automatic seedpoint selection later on, the region containing the optic nerve (ON) and its sheath was localized and extracted from the original B-mode image. Hereto, a black-white image was created using a threshold of .26 [–] (Figs 1A and 1B). Next, the distal part of the globe and the corresponding retrobulbar structures were extracted by searching for the boundaries of the largest object within this image. This was done by locating the first and last white pixel for each row and column within the image (Fig 1B). Next, an estimation of the ON location was made by searching for the vertical B-mode intensity line with the most black pixels. Thereafter, the nerve midpoint, that is, the intersect between this intensity line and the retina, was determined. Subsequently, the image was cropped in the x- and y-direction using an arbitrary chosen width of 12 mm around the ON location and a height corresponding to a depth of 10 mm from the retina, respectively (Fig 1C). Next, the pixels corresponding to the retina were detected by a search for the first white pixel within each of the vertical B-mode intensity lines followed by the fitting of a second order polynomial curve through these points (Fig 1D).

### Step 2: Image enhancement

In high-quality images, the hyperechoic bands are separated from the hyperechoic retrobulbar fat by a thin dark line. In practice, this dark line is not always clearly visible causing the hyperechoic bands and retrobulbar fat to blend into each other, which hampers accurate detection of the outer border of the hyperechoic striped bands. Therefore, we first enhanced the image to increase the contrast between these two structures. Hereto, we applied a 2-dimensional Butterworth bandpass filter with cutoff frequencies of 5 and 10 Hz, respectively (Fig 1E). Subsequently, the image was sharpened by the subtraction of a Gaussian blurred image ($\mu = 0$ and $\sigma = 20$ pixels) from the bandpass-filtered image (Fig 1F).

Step 3: Feature calculation

Despite image enhancement, segmentation of structures in ultrasound images can still be difficult due to, for example, small or no differences in intensities between structures of interest or the presence of speckle or artifacts that mask the outlines of structures.[20] To overcome this intensity dependency, we chose to detect the borders of the structures of interest using Kovesi's signed asymmetry features calculated from the monogenic signal of the image. These asymmetry features have values between −1 and +1, where values close to −1 or 1 correspond
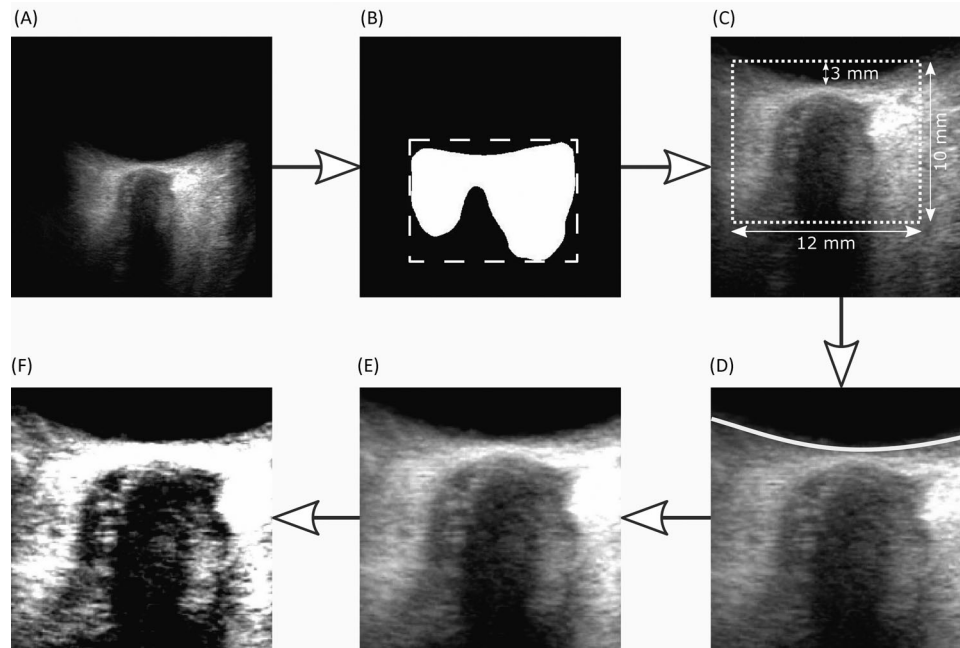
FIGURE 1 Region of interest selection and image enhancement. (A) Original B-mode ultrasound image. (B) Detection of the outline of the retrobulbar structures used for the initial image crop. (C) Detection of the optic nerve midpoint, that is, crossing of the nerve midline and the retina (white arrow). Next the image is cropped using a width of 12 mm and a depth of 10 mm around the nerve midpoint. (D) Retina detection and fitting of a second-order polynomial (white line). (E) Bandpass filtering of the cropped image. (F) Image enhancement of the bandpass filtered image
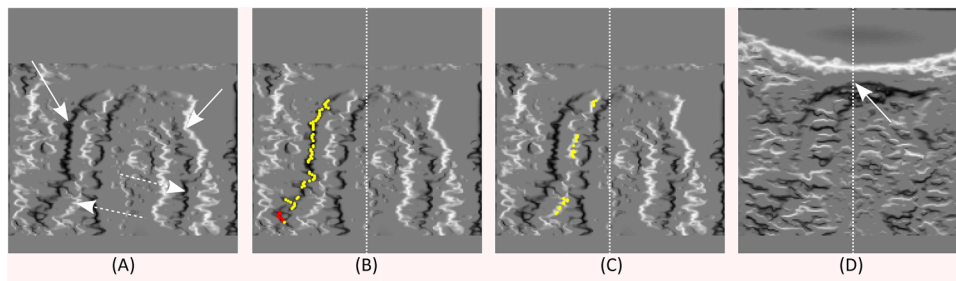

FIGURE 2 (A) Signed asymmetry features of the enhanced cropped image. The borders corresponding to the retrobulbar fat and the hyperechoic bands are indicated by white solid arrows and dotted arrows, respectively. (B and C) Detection of the edges corresponding to the border of the retrobulbar fat and the hyperechoic bands, respectively. Yellow points denote the found edges, whereas red points denote outliers. (D) Detection of the edge corresponding to the "dome" of the nerve (white arrow). The white dotted line denotes the vertical midline of the optic nerve

to "changes" that are, respectively, troughs or peaks (Fig 2). For more information about the monogenic signal, we refer the reader to Bridge et al.[21]

The signed asymmetry features were derived from the monogenic signal calculated using wavelengths $(\lambda_i) = 12^i$ in mm with $i = 0, 1, \ldots, 6$, bandpass-shape parameter $\sigma_0 = .35$,[21] and a scale-specific noise threshold T of .18.[21] An example of the x-directed signed asymmetry features for one of our images can be seen in Fig 2A. As can be seen in Fig 2A, the left border of the hyperechoic band is a peak (white = positive), whereas the left border of the fat is a trough (black = negative).

Step 4: Initial fat and sheath detection

The next step was the detection of the external outlines of the hyperechoic striped bands and the internal outline of the hyperechoic retrobulbar fat. Initial points corresponding to the outline of the retrobulbar fat and sheath were located. Hereto, we performed a row-wise search starting from the middle of the image toward the left side of the image and annotated the first peak after a trough as "sheath" and the second trough in each row as "fat" (Figs 2B and 2C). Subsequently, we removed possible outliers by detecting and removing points that deviated more than three standard deviations from the median. The right side edges of
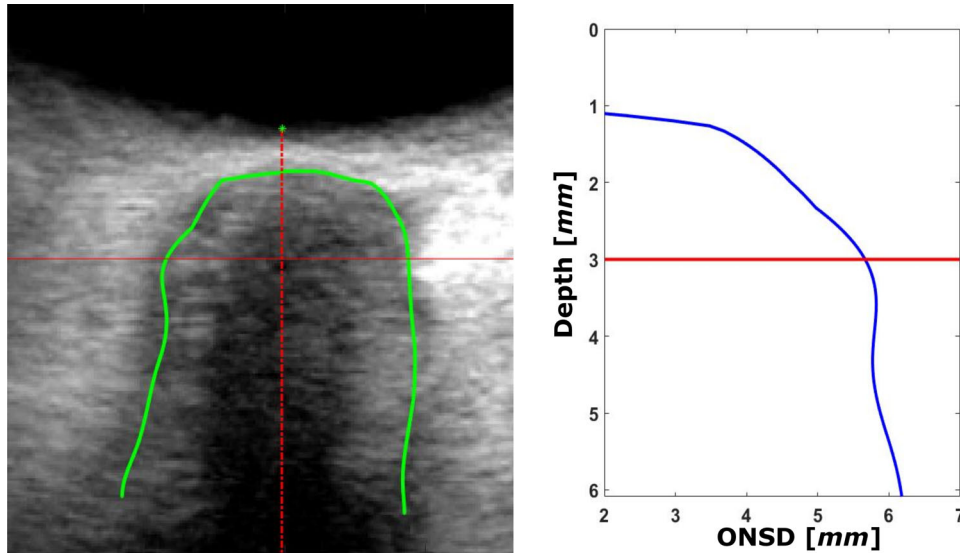
FIGURE 3 Final delineation of the optic nerve and its sheath (left). The corresponding optic nerve sheath diameter (ONSD) as function of the depth (right)

the hyperechoic band and fat were detected in the same way but taking into account the change of sign.

To obtain a better estimation of the sheath outline at the top of the nerve, we also wanted to segment the "dome of the nerve" in the next stage. Hereto, we determined a point located at the edge of the dome by finding the crossing of the nerve midline with the first trough found from the retina down on the y-directed signed asymmetry image (see Fig 2D).

Step 5: Segmentation

To obtain a better estimate of the edges and to allow detection of the borders on locations where no initial outline was found, we evolved a contour along the edges of interest. We used the localized active contour as described by Lankton et al[22] and implemented by Pang et al,[23] hereby using the annotated points from the previous step as initialization for the contour.

Using the active contour, the sheath, fat, and dome were segmented, hereby choosing a penalty constant of .05 for the sheath and the fat, and .3 for the dome segmentation, and a mask radius of 20 pixels. To control the computational time of the gradient-descent method used to minimize the energy of the contour, the maximum number of iterations was set to 100, 400, and 150 for sheath, fat, and dome, respectively.

Step 6: ONSD calculation

After the contours for the sheath, fat, and dome were evolved, an initial outline of the optic nerve and the sheath was determined. Hereto, the inner edges of the fat segmentation and the outer edges of the sheath segmentation were localized at multiple depths perpendicular to the nerve midline. When no sheath outline was found at a given depth,

the fat outline at that depth was used instead. In addition, the superior edge of the dome contour was detected by a search in the vertical direction. Subsequently, all outline points were combined into one curve and smoothed with a smoothing spline ("smoothn" function in Matlab with a high smoothing parameter). Finally, the ONSD was calculated at multiple depths by taking the distance between the left and right outline (see Fig 3). The complete automated ONSD estimation takes between 30 and 60 seconds per image on a personal laptop.

Assessment of the algorithm performance

To assess the quality of the automated ONSD algorithm, we compared the automatic algorithm-derived ONSD values with ONSD values from manual assessments performed by two human experts (Operator 1 and Operator 2). These experts were not involved in the image acquisition but solely determined the ONSD on these images. Manual assessments by the experts were performed in Matlab using an in-house-developed framework built such that it resembled ONSD segmentation on a real ultrasound scanner as closely as possible. Both experts analyzed the 42 ultrasound images twice in unknown order while blinded to any patient information.

First of all, we assessed the intraobserver variability, that is, the agreement between ONSD values obtained when the same image is analyzed twice by the same rater, for each expert and for the automated algorithm. Hereto, we calculated the coefficient of determination (R^2) for the linear regression model $y = x$, where x and y represent the first and second measurement (M1 and M2), respectively. In addition, we determined the mean difference and limits of agreement using Bland-Altman plots. Logically, the intraobserver variability of the algorithm is zero as the algorithm yields the same ONSD value every time the same image is analyzed.

TABLE 1 Optic Nerve Sheath Diameters Obtained with the Algorithm and by the Two Operators

ONSD	Algorithm	Operator 1	Operator 2
First measurements	5.42 ± .54	5.30 ± .40	5.40 ± .46
Second measurements		5.38 ± .54	5.34 ± .50
Averaged measurements		5.34 ± .47	5.37 ± .45

Data represents mean ± standard deviation of the optic nerve sheath diameter (ONSD) values (mm) obtained with the algorithm and by the two operators. No significant differences ($P > .05$) were found between the algorithm and the experts using the Wilcoxon signed rank test.

Second, we examined the interobserver variability, that is, the agreement between ONSD values obtained when the same image is analyzed by two different raters, between the experts and the algorithm, and between the experts themselves. However, two different analyses were carried out. In the first analysis, we calculated the mean of the two repeated manual ONSD assessments for each expert (mOp1 and mOp2) and compared these values between the two experts (mOp1 – mOp2) and with the ONSD values derived by the algorithm (mOp1 – A and mOp2 – A). In the second analysis, we only considered the first measurement of the operators (Op1 and Op2) to evaluate the effect of repeated measurements and to enable comparison with reported results in literature that were based on single measurements. Similarly as for the intraobserver variability, linear regression models $y = x$ were made for each analysis, that is, for the comparisons between Operator 1 and the algorithm, Operator 2 and the algorithm, and Operator 1 and Operator 2. Subsequently, the corresponding coefficients of determination were calculated. Moreover, the corresponding mean difference and limits of agreement were derived from Bland-Altman plots. Finally, we investigated if the mean ONSD values of the Algorithm, Operator 1, and Operator 2 were statistically different, hereby using the Wilcoxon signed rank test because the data were not normally distributed. Statistical analysis was performed in Matlab (R2018a, The MathWorks, Inc., Natick, Massachusetts, United States).

RESULTS

Accurate segmentation of the B-mode ultrasound images was possible in 39 out of the 42 images, resulting in a success rate of almost 93%. In two images, the segmentation clearly failed because of a dark image artifact just below the retina that masked the true outline of the hyperechoic band and retrobulbar fat on one side, whereas in another image the physical orientation of the optic nerve deviated largely from the vertical midline assumed in our algorithm, resulting in a very large ONSD value. In contrast to the algorithm, the experts were able to obtain ONSD values in these three images by means of extrapolation. However, for comparison between the automated and the manual ONSD assessments these three images were excluded from further analysis.

The means and standard deviations of the ONSD calculated over all the images are given in Table 1. Although the mean ONSD value of the algorithm is slightly higher than the ONSD values derived by the experts, these differences were found to be nonsignificant.

The Bland-Altman plots used to analyze the interobserver variabilities between the averaged repeated ONSD measurements of Operator 1 (mOp1), Operator 2 (mOp2), and the ONSD values obtained with the algorithm (A) are given in Figure 4 and in Table 2. The ONSD values determined by the automatic algorithm were on average slightly higher than the manually derived values, that is, mean differences of −.08 ± .45 and −.05 ± .41 mm when compared with the averaged manual expert assessments of Operator 1 and Operator 2, respectively. In comparison, Operator 1 showed a mean difference of −.03 ± .26 mm with respect to Operator 2. In addition, the corresponding R^2-values are .37, .44, and .71 for Operator 1 versus Algorithm, Operator 2 versus Algorithm, and Operator 1 versus Operator 2, respectively.

The interobserver variabilities of the comparison between the first measurement of Operator 1 (Op1), Operator 2 (Op2), and the algorithm (A) are also given in Table 2. Comparing only the first manual measurements slightly increased the interobserver variabilities between the observers and the algorithm to −.12 ± .47 and −.02 ± .41 mm for Operator 1 and Operator 2, respectively, whereas the difference between the experts increased to −.1 ± .30 mm.

The intraobserver variabilities of Operator 1 and Operator 2 are shown in Figure 5. The first measurements of Operator 1 showed a mean difference of −.08 ± .33 mm compared to the second measurements. In addition, the first measurements of Operator 2 showed a mean difference of .06 ± .30 mm compared to the second measurements. The corresponding R^2-values were .63 for Operator 1 and .65 for Operator 2. Obviously, the algorithm has no intraobserver variability because the algorithm yields exactly the same ONSD value when the same image is analyzed twice.

## DISCUSSION

Major findings

In this study, we developed an algorithm that allows for automatic ONSD assessment from B-mode ultrasound images. Using asymmetry features, we were able to segment the ONSD at a range of depths in 93% of the images in which the sheath outline was often poorly visible.

To validate the ONSD values obtained with the algorithm, these values were compared to manual ONSD assessements performed by two experts. The intraobserver variability of both our operators (.33 and .30 mm) was only a bit larger than the ones reported by Bäuerle et al[8] (.22 mm) and the R^2 of both operators was comparable to the values reported in two studies of Bäuerle et al,[8,16] indicating representative expert assessments.

Mean ONSD values derived by the algorithm were slightly higher than the mean ONSD values derived by the experts; however, these differences were not statistically significant and the ONSD values were within clinically observed ranges, indicating that the algorithm-derived ONSD values were representative for the clinical situation.

FIGURE 4 Bland-Altman plots comparing the automatic optic nerve sheath diameter (ONSD) with the manual assessments by Operator 1 (A), and the manual assessments by Operator 2 (B), and comparing the manual assessments by Operator 1 with manual assessments by Operator 2 (C). Solid lines depict the mean of the differences and dashed lines denote the limits of agreement. Moreover, mOp1 and mOp2 denote the averaged ONSD value of repeated measurements performed by Operator 1 and Operator 2, respectively
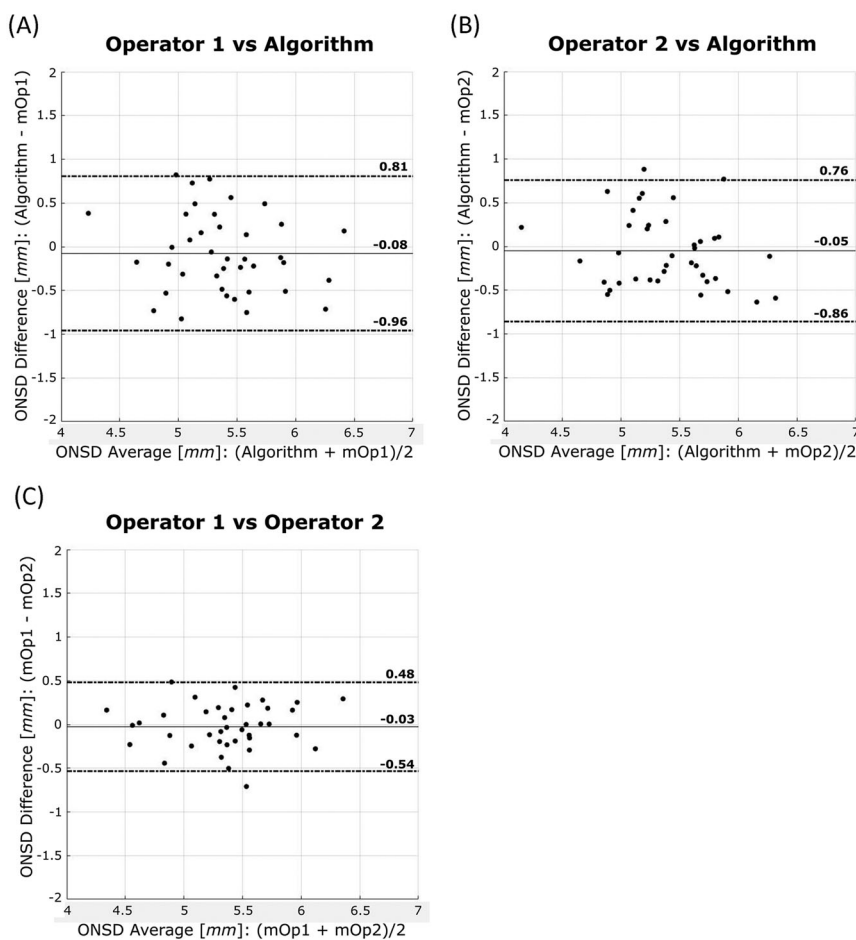
The interobserver variabilities obtained in our study and the ones found in literature are given in Table 2. Overall, the interobserver variabilities between the two experts found in this study are comparable with values reported in literature. The interobserver variabilities between the experts and the algorithm are a bit larger than our interobserver variabilities between the two experts; however, similarly as Meiburger et al,[19] the difference between expert-derived ONSD values and algorithm-derived ONSD values is much smaller than the 1 mm differences in ONSD values between patients with normal and elevated ICP reported in literature.[24–26] This makes it likely that our algorithm can detect differences in ONSD values between patients with elevated ICP and patients with normal ICP. Also, use of an automated algorithm is not subject to observer variability and therefore the objective detection of elevated ICP compared to normal ICP based on a cutoff value could be more accurate.

Compared to the algorithm presented by Meiburger et al,[19] we found a slightly smaller interobserver variability between the ONSD values derived with the algorithm and the expert ONSD values, whereas the R^2s of the linear regression between our algorithm and experts were comparable to the values reported by Meiburger et al.[19] Similarly as Meiburger et al,[19] our approach allows segmentation of the outline of the optic nerve sheath when the hyperechoic bands are noncontinuous, that is, not visible on every depth. In contrast to Meiburger et al,[19] our intensity-invariant features enable us to also segment the

outline of the optic nerve sheath when the thin dark line separating the retrobulbar fat and the hyperechoic bands is poorly visible, that is, the retrobulbar fat and hyperechoic bands blend into each other. Moreover, our algorithm is not hindered by differences in image intensities due to discrepancies in, for example, ultrasound machine settings. This facilitates the deployment of the algorithm in different clinical centres.

The comparison between single and repeated ONSD measurements shows that ONSD measurements performed by two observers deviate more from each other when these ONSD values are obtained using nonrepeated measurements. In line with this observation, most studies calculate the mean of multiple ONSD measurements. This, however, increases the time it takes to perform manual ONSD measurements.[19] Similarly as the algorithm of Meiburger et al,[19] our algorithm has no intrinsic variability and therefore one singular measurement is sufficient to obtain an accurate ONSD value. This does not only reduce the time it takes to perform ONSD assessments but also overcomes the variation within the ONSD values due to intra- and interobserver variabilites associated with manual ONSD assessment.

Limitations and future work

Our study has a few limitations. Most important is the fact that we did not investigate if our algorithm does indeed lead to a more accurate

TABLE 2 Comparison of the Interobserver Variability Found in Literature and the Current Study

Author	Comparison	Bias	SD	LOA		R^2
Lochner et al[9]	Op1 – Op2 (L)	.08	.28	.48	–.64	–
	Op1 – Op2 (R)	.09	.40	.71	–.90	–
Bauerle et al[16]	Op1 – Op2	.25	.51	1.25	–.75	.67
Bauerle et al[8]	Op1 – Op2 (L)	.10	.38	.84	–.64	.66
	Op1 – Op2 (R)	.04	.37	.77	–.69	.71
Meiburger et al[19]	Op1 – Op2	.44*	.52	1.46	–.58	.42
	Op1 – A	.06	.52	1.07	–.95	.41
	Op2 – A	–.38	.55	.69	–1.44	.37
Our work	mOp1 – mOp2	–.03	.26	.48	–.54	.71
	mOp1 – A	–.08	.45	.81	–.96	.37
	mOp2 – A	–.05	.41	.76	–.86	.44
	Op1 – Op2	–.10	.30	.48	–.67	.63
	Op1 – A	–.12	.47	.81	–1.04	.31
	Op2 – A	–.02	.41	.78	–.82	.46

SD and LOA denote standard deviation and limits of agreement, respectively. In addition, mOp1 and mOp2 denote the average of repeated manual optic nerve sheath diameter (ONSD) measurements performed by Operator 1 and Operator 2, respectively, whereas Op1 and Op2 denote that only the first ONSD measurements of Operator 1 and Operator 2 are considered, respectively. Furthermore, the letter A stands for Algorithm and the letters L and R denote measurements of the left or right eye only.
*The large bias is most likely caused because Op1 was experienced, whereas Op2 was less experienced.

detection of elevated ICP. Although our algorithm eliminates the intra- and interobserver variabilities present within the manually derived ONSD values, automated ONSD assessment might not be enough to obtain accurate ONSD cutoff values for the detection of elevated ICP

because the inconsistencies in manual delineation of the optic nerve sheath only represent part of the methodological differences reported in literature.[12,14,27,28] Also differences in image acquisition, such as the ultrasound machine, and the experience of the operator can have an impact on the ONSD values. In order to obtain more accurate ONSD values, it is therefore necessary to not only utilize automatic segmentation algorithms, but also to standardize the transocular ultrasound acquisition.[14,19]

Moreover, for now we assumed the nerve midline to be vertically oriented. Though the optic nerve was orientated approximately vertical in most of our ultrasound images, it would be more accurate to calculate the ONSD using a correctly angled optic nerve midline. This would also allow us to obtain correct ONSD values from images with a very tilted optic nerve, such as the image we now excluded. This will probably further improve the agreement with the expert ONSD values.

Another limitation is that the automatic segmentation failed in two images because a dark image artifact below the retina obscured the outline of the hyperechoic band and the retrobulbar fat. Where, in such cases, the human brain is able to approximate these edges using information from regions where this distinction is visible, the algorithm is not able to correctly estimate these edges. Nevertheless, these manual approximations are also subject to observer variability. Although our algorithm should be improved to allow more accurate extrapolation in such images, mimicking the extrapolation capabilities of the human brain is not easy. Though one could resort to machine learning, the performance of such algorithms is highly dependent on the quality and number of images used to train the machine learning algorithm.[29]

In this study, the ultrasound images had to be exported for offline analysis. Although exporting images is relatively easy, this extra step might limit the use of automated ONSD algorithms in the clinic. It might therefore be useful to incorporate the algorithm in ultrasound machines, making it available while performing transocular sonography. Implementing algorithms on commercial devices is often not possible without involvement of the manufacturer but should be
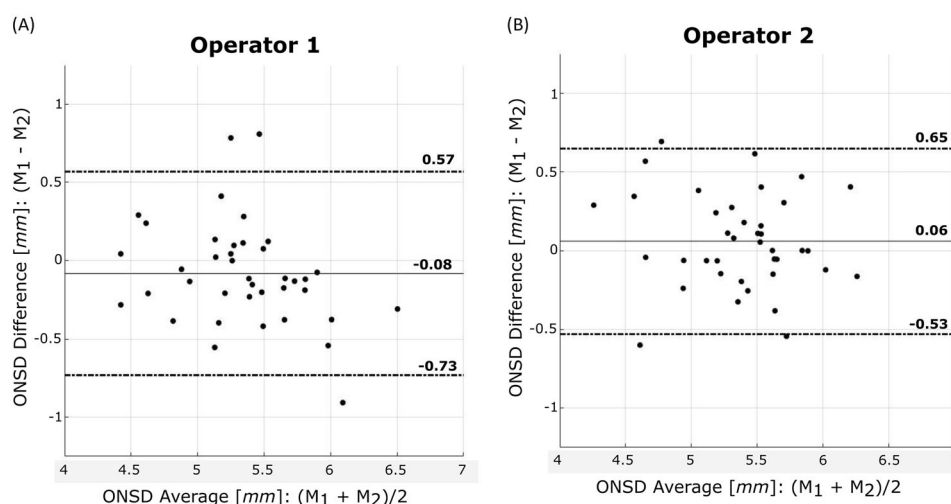
FIGURE 5 Bland-Altman plots comparing the repeated optic nerve sheath diameter (ONSD) measurements (M1 and M2) for Operator 1 (A) and Operator 2 (B). Solid lines depict the mean of the differences and dashed lines denote the limits of agreement

encouraged because it can increase the application of automated ONSD estimation in the clinical setting.

Improving the accuracy of ONSD estimation is not the only use of our algorithm. Because our algorithm yields ONSD values not only at the conventionally used 3 mm but also at a wide range of other depths, it allows us to investigate the sensitivity of ONSD to changes in ICP at multiple depths. This might give answer to the question if ONSD assessment at 3 mm is the best practice in all patients.[30,31] Moreover, the use of transocular ultrasonography is not limited to the assessment of elevated ICP but can also be used to aid in the diagnosis and follow-up of patients with intracranial hypotension[32] or idiopathic normal pressure hydrocephalus.[33] Moreover, there are also studies that report the assessment of optic nerve diseases such as in multiple sclerosis[34,35] by measuring swelling of the optic nerve and the ONSD. Also in these cases, automated algorithms can be used to reduce the variability associated with manual assessments.

In conclusion, we developed an automated intensity-invariant algorithm capable of estimating the ONSD from B-mode ultrasound images. The ONSD derived with the algorithm showed good agreement with manual expert assessments. Moreover, the differences between the automatically and manually derived ONSD values were within the ranges of interobserver variabilities reported in literature. Because the algorithm has no intrinsic variability, it eliminates the intra- and inter-observer variabilities in ONSD values associated with manual ONSD assessment. Therefore, we believe that our algorithm can be used to derive more accurate ONSD cutoff values for the detection of elevated ICP.

ORCID

Raoul R. F. Stevens https://orcid.org/0000-0003-1860-2846

REFERENCES

1. Hansen HC, Helmke K. Validation of the optic nerve sheath response to changing cerebrospinal fluid pressure: ultrasound findings during intrathecal infusion tests. J Neurosurg 1997;87:34-40.
2. Geeraerts T, Merceron S, Benhamou D, et al. Non-invasive assessment of intracranial pressure using ocular sonography in neurocritical care patients. Intensive Care Med 2008;34:2062-7.
3. Toscano M, Spadetta G, Pulitano P, et al. Optic nerve sheath diameter ultrasound evaluation in intensive care unit: possible role and clinical aspects in neurological critical patients' daily monitoring. Biomed Res Int 2017;2017:1621428.
4. Soldatos T, Karakitsos D, Chatzimichail K, et al. Optic nerve sonography in the diagnostic evaluation of adult brain injury. Crit Care 2008;12:1-7.
5. Ertl M, Weber S, Hammel G, et al. Transorbital sonography for early prognostication of hypoxic-ischemic encephalopathy after cardiac arrest. J Neuroimaging 2018;28:542-8.
6. Siepen BM, Grubwinkler S, Wagner A, et al. Neuromonitoring using neurosonography and pupillometry in a weaning and early neurorehabilitation Unit. J Neuroimaging 2020;30:631-9.
7. Hansen HC, Helmke K. The subarachnoid space surrounding the optic nerves. An ultrasound study of the optic nerve sheath. Surg Radiol Anat 1996;18:323-8.
8. Bäuerle J, Lochner P, Kaps M, et al. Intra- and interobsever reliability of sonographic assessment of the optic nerve sheath diameter in healthy adults. J Neuroimaging 2012;22:42-5.
9. Lochner P, Coppo L, Cantello R, et al. Intra- and interobserver reliability of transorbital sonographic assessment of the optic nerve sheath diameter and optic nerve diameter in healthy adults. J Ultrasound 2014;19:41-5.
10. Dubourg J, Javouhey E, Geeraerts T, et al. Ultrasonography of optic nerve sheath diameter for detection of raised intracranial pressure: a systematic review and meta-analysis. Intensive Care Med 2011;37:1059-68.
11. Wang LJ, Yao Y, Feng LS, et al. Noninvasive and quantitative intracranial pressure estimation using ultrasonographic measurement of optic nerve sheath diameter. Sci Rep 2017;7:42063.
12. Pichamuthu KK, Prithishkumar IJ. Appearance of the optic nerve sheath diameter (ONSD) using higher frequency linear probes in detection and monitoring of raised intracranial pressures-a cadaveric study. J Clin Diagnostic Res 2019;13:5-8.
13. Schroeder C, Katsanos AH, Richter D, et al. Quantification of optic nerve and sheath diameter by transorbital sonography: a systematic review and metanalysis. J Neuroimaging 2020;30:165-74.
14. Bloria S, Bloria P, Luthra A. Is it the time to standardize the procedure of ultrasound guided optic nerve sheath diameter measurement? Saudi J Anaesth 2019;13:255-6.
15. Topcuoglu MA, Arsava EM, Bas DF, et al. Transorbital ultrasonographic measurement of optic nerve sheath diameter in brain death. J Neuroimaging 2015;25:906-9.
16. Bäuerle J, Schuchardt F, Schroeder L, et al. Reproducibility and accuracy of optic nerve sheath diameter assessment using ultrasound compared to magnetic resonance imaging. BMC Neurol 2013;13:187.
17. Gerber S, Jallais M, Greer H, et al. Automatic estimation of the optic nerve sheath diameter from ultrasound images. Imaging Patient Cust Simul Syst Point Care Ultrasound 2017;10549:113-20.
18. Soroushmehr R, Rajajee K, Williamson C, et al. Automated optic nerve sheath diameter measurement using super-pixel analysis. Annu Int Conf IEEE Eng Med Biol Soc 2019;2019:2793-6.
19. Meiburger KM, Naldi A, Michielli N, et al. Automatic optic nerve measurement: a new tool to standardize optic nerve assessment in ultrasound B-mode images. Ultrasound Med Biol 2020;46:1533-44.
20. Rackham TM, Rueda S, Knight CL, et al. Ultrasound image segmentation using feature asymmetry and shape guided live wire. Proc. SPIE 8669, Medical Imaging 2013 https://doi.org/10.1117/12.2007131.
21. Bridge CP. Introduction to the monogenic signal. Available at: https://arxiv.org/abs/1703.09199. Accessed December 6, 2018.
22. Lankton S, Tannenbaum A. Localizing region-based active contours. IEEE Trans Image Process 2008;17:2029-39.
23. Pang J. Localized active contour. Available at: www.mathworks.com/matlabcentral/fileexchange/44906-localized-active-contour. Accessed July 21, 2020.
24. Lochner P, Fassbender K, Lesmeister M, et al. Ocular ultrasound for monitoring pseudotumor cerebri syndrome. J Neurol 2018;265:356-61.
25. Moretti R, Pizzi B, Cassini F, et al. Reliability of optic nerve ultrasound for the evaluation of patients with spontaneous intracranial hemorrhage. Neurocrit Care 2009;11:406-10.
26. Lochner P, Cantello R, Fassbender K, et al. Longitudinal assessment of transorbital sonography, visual acuity, and biomarkers for inflammation and axonal injury in optic neuritis. Dis Markers 2017;2017:5434310.
27. Ballantyne SA, O'Neill G, Hamilton R, et al. Observer variation in the sonographic measurement of optic nerve sheath diameter in normal adults. Eur J Ultrasound 2002;15:145-9.
28. Copetti R, Cattarossi L. Optic nerve ultrasound: artifacts and real images. Intensive Care Med 2009;35:1488-9.
29. Cantisani V, Grani G, Tovoli F, et al. Artificial intelligence: what is it and how can it expand the ultrasound potential in the future? Ultraschall Med 2020;41:356-60.

30. Vaiman M, Sigal T, Kimiagar I, et al. Intracranial pressure assessment in traumatic head injury with hemorrhage via optic nerve sheath diameter. J Neurotrauma 2016;33:2147-53.

31. Vaiman M, Gottlieb P, Bekerman I. Quantitative relations between the eyeball, the optic nerve, and the optic canal important for intracranial pressure monitoring. Head Face Med 2014;10:1-6.

32. Fichtner J, Ulrich CT, Fung C, et al. Management of spontaneous intracranial hypotension - transorbital ultrasound as discriminator. J Neurol Neurosurg Psychiatry 2016;87:650-5.

33. Ertl M, Aigner R, Krost M, et al. Measuring changes in the optic nerve sheath diameter in patients with idiopathic normal-pressure hydrocephalus: a useful diagnostic supplement to spinal tap tests. Eur J Neurol 2017;24:461-7.

34. De Masi R, Orlando S, Conte A, et al. Transbulbar B-mode sonography for clinical phenotyping multiple sclerosis. Appl Sci 2018;8:1-12.

35. Lochner P, Leone MA, Coppo L, et al. B-mode transorbital ultrasononography for the diagnosis of acute optic neuritis: a systematic review. Clin Neurophysiol 2016;127:803-9.